PHILOSOPHICAL TRANSACTIONS OF THE ROYAL SOCIETY A

Phil. Trans. R. Soc. A (2011) **369**, 4605–4619
doi:10.1098/rsta.2011.0271

In vivo Cerenkov luminescence imaging: a new tool for molecular imaging

By Gregory S. Mitchell*, Ruby K. Gill, David L. Boucher, Changqing Li and Simon R. Cherry

Department of Biomedical Engineering, and Center for Molecular and Genomic Imaging, University of California at Davis, One Shields Avenue, Davis, CA 95616, USA

Cerenkov radiation is a phenomenon where optical photons are emitted when a charged particle moves faster than the speed of light for the medium in which it travels. Recently, we and others have discovered that measurable visible light due to the Cerenkov effect is produced *in vivo* following the administration of β-emitting radionuclides to small animals. Furthermore, the amounts of injected activity required to produce a detectable signal are consistent with small-animal molecular imaging applications. This surprising observation has led to the development of a new hybrid molecular imaging modality known as Cerenkov luminescence imaging (CLI), which allows the spatial distribution of biomolecules labelled with β-emitting radionuclides to be imaged *in vivo* using sensitive charge-coupled device cameras. We review the physics of Cerenkov radiation as it relates to molecular imaging, present simulation results for light intensity and spatial distribution, and show an example of CLI in a mouse cancer model. CLI allows many common radiotracers to be imaged in widely available *in vivo* optical imaging systems, and, more importantly, provides a pathway for directly imaging β^--emitting radionuclides that are being developed for therapeutic applications in cancer and that are not readily imaged by existing methods.

Keywords: Cerenkov radiation; optical imaging; *in vivo* molecular imaging

1. Optical molecular imaging

In vivo molecular imaging involves the non-invasive interrogation of living subjects with a general goal of providing images that directly relate to the spatial and the temporal distributions of expression levels of specific genes or proteins. Techniques to image a variety of protein targets (including receptors, transporters and enzymes) and to image the regulation of gene expression have been developed across multiple imaging modalities, including optical imaging, nuclear imaging and magnetic resonance imaging [1,2]. Furthermore, a major emphasis has been placed on developing techniques that allow the pharmacokinetics of new therapeutic entities to be imaged, or that permit the action of a therapeutic entity on its intended target to be monitored [3].

*Author for correspondence (gsmitchell@ucdavis.edu).

One contribution of 20 to a Theo Murphy Meeting Issue 'Illuminating the future of biomedical optics'.

Optical imaging is one of the most sensitive molecular imaging techniques, and is especially suited for preclinical studies in mice, where light in the near-infrared part of the spectrum can readily reach the surface of the animal, even when produced inside the deepest tissues. Techniques for imaging gene expression *in vivo* have been developed using optical reporters, such as firefly luciferase (which results in bioluminescence in the presence of its substrate luciferin) [4] and red fluorescent reporter proteins [5]. An increasing range of fluorescently labelled contrast agents have also been developed with molecular targeting for a variety of receptors and enzymes [6]. While reporter genes and fluorescent labelling agents are important techniques for small-animal imaging, they cannot typically be translated to clinical practice.

We report here on a new source of optical contrast that can be exploited for molecular imaging studies based on the emission of visible light produced via the Cerenkov effect from biomolecules labelled with β-emitting radionuclides. This allows many common (and clinically relevant or useful) radiotracers to be imaged in widely available *in vivo* optical imaging systems, and, more importantly, provides a pathway for directly imaging β^--emitting radionuclides that are being developed for therapeutic applications in cancer and that are not readily imaged by the existing methods. Initial published reports that characterize the use of Cerenkov light for molecular imaging are given in earlier studies [7–10].

2. Cerenkov radiation for molecular imaging: theory and simulations

Cerenkov radiation, most commonly encountered as the source of the blue glow of a nuclear reactor, was discovered decades ago [11], and a thorough theoretical treatment was provided by Frank and Tamm soon thereafter, as summarized by Jelley [12]. A moving charged particle travelling in a dielectric will slightly polarize the molecules of the medium; as they return to their ground state, the molecules emit prompt radiation. Cerenkov radiation is a threshold effect: when the velocity of the particle, v, is greater than c/n (the speed of light in a vacuum divided by the index of refraction of the medium), there is a well-defined angle with respect to the particle's trajectory at which the particle induces coherent electromagnetic radiation with a continuous spectrum. The constructive interference at this angle results in an observable number of visible Cerenkov photons. The intensity of the radiation depends on the velocity, and therefore the energy, of the particle, and also increases in materials with higher refractive index. The Cerenkov angle, $\cos\theta = 1/(vn/c)$, with respect to the particle velocity direction, is dependent on the velocity, and thus the emission direction will change if the particle slows down as a result of scattering-induced energy losses.

The production of Cerenkov light is described by the Frank–Tamm formula, which gives the number of photons N per distance travelled x:

$$\frac{\mathrm{d}N}{\mathrm{d}x} = 2\pi\alpha\left(1 - \frac{1}{\beta^2 n^2}\right)\int_{\lambda_1}^{\lambda_2} \frac{1}{\lambda^2}\mathrm{d}\lambda, \tag{2.1}$$

where α is the dimensionless fine-structure constant (1/137), n is the index of refraction and β is the ratio of the particle velocity to the speed of light, v/c.

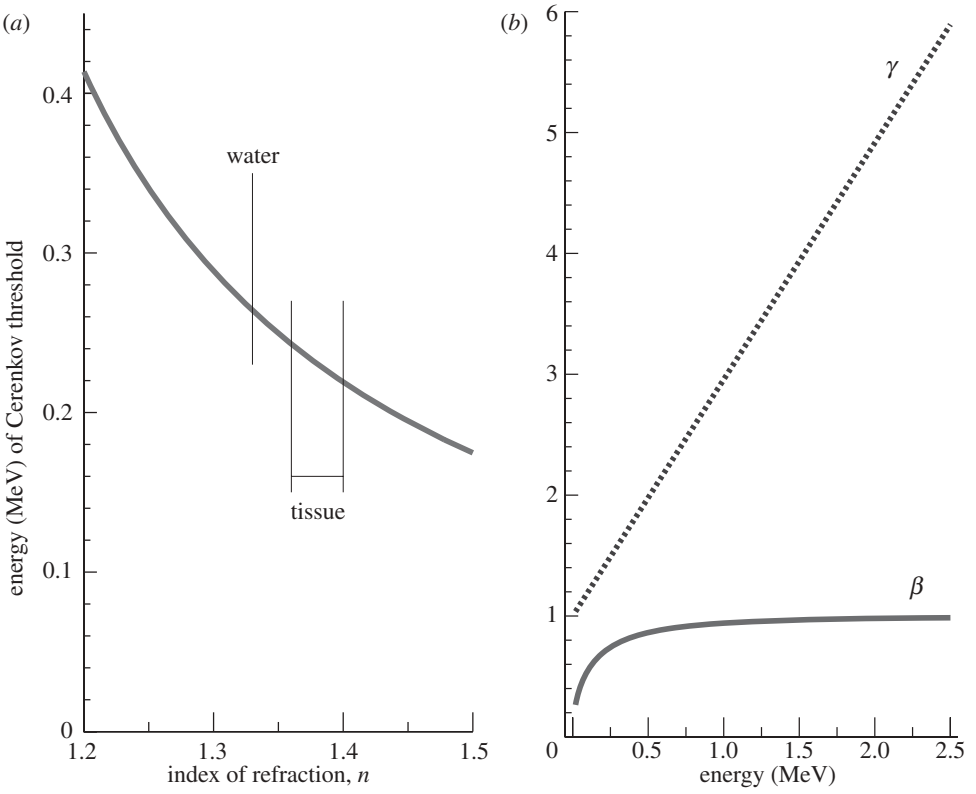

Figure 1. (*a*) Threshold β-particle energy for production of Cerenkov radiation as a function of refractive index. (*b*) Values of the dimensionless parameters β and γ (equations (2.1) and (2.3)) as a function of the kinetic energy of a β-particle.

(Note that there exists an unfortunate confusion of the conventional notation for this quantity with the notation for radioactive decay via electron or positron emission.) The integral is over the range of observed wavelengths λ_1 to λ_2.

As shown by equation (2.1), the spectral distribution of the Cerenkov light is inversely proportional to the square of the wavelength. Thus, the peak of the emitted photon spectrum in the visible light range is at blue wavelengths. However, there are detectable photons even at the longer wavelengths (700–900 nm) associated with good tissue penetration for *in vivo* optical imaging. At shorter (UV) wavelengths, media typically have increased absorption and scattering of light (are no longer transparent). The index of refraction, which is wavelength–dependent, becomes less than 1 at X-ray energies, and thus there is no Cerenkov emission at these short wavelengths.

Cerenkov radiation has a threshold for production, expressed as $\beta n > 1$. In water, which has a refractive index of 1.33 in the visible spectrum, the threshold for the production of Cerenkov light for a β-particle is 0.263 MeV. In tissue, where the index of refraction is more typically around 1.36–1.40, this threshold is reduced to approximately 0.21–0.24 MeV (figure 1*a*). The vast majority of β-emitting radionuclides of biomedical interest, including all the

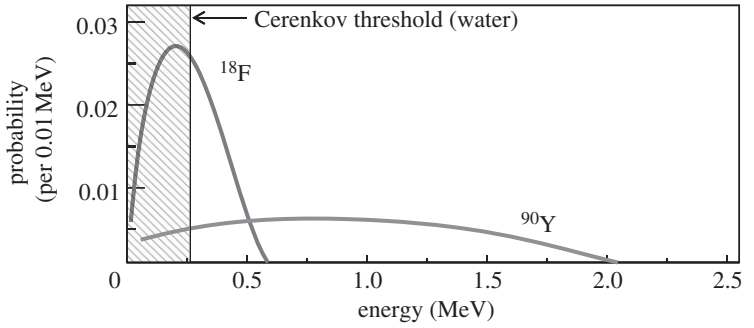

Figure 2. Spectrum of emitted β-particle energies for the radionuclides ^{18}F (endpoint energy 0.633 MeV) and ^{90}Y (endpoint energy 2.28 MeV). The Cerenkov threshold for β-particles in water (0.263 MeV) is also shown; no Cerenkov radiation is produced for this (shaded) portion of the decay spectrum. (Based on data available at www.doseinfo-radar.com/RADARDecay.html.)

positron-emitting radionuclides used in positron emission tomography (PET), have endpoint energies significantly higher than these thresholds and therefore produce detectable Cerenkov light in water or in tissue [8]. We note that Cerenkov light has previously been used quantitatively for *in vitro* applications [13,14] and more recently to monitor a microfluidics apparatus [15].

To estimate and understand the intensity of the light emission, we consider the various factors in equation (2.1). As an example, for the commonly used PET radionuclide ^{18}F, the positrons produced upon radioactive decay have an endpoint (maximum) kinetic energy of 633 keV and a most probable value of approximately 250 keV. Relativistic kinetic energy (E) is given by (e.g. [16])

$$E = mc^2 - m_0 c^2 = m_0 c^2(\gamma - 1), \tag{2.2}$$

where m_0 is the rest mass of the particle, which for an electron or positron is 511 keV c^{-2}, and where

$$\gamma = \frac{1}{(1-\beta^2)^{1/2}}. \tag{2.3}$$

Figure 1*b* graphically shows the relationships between the dimensionless parameters β and γ and the kinetic energy of the positrons or electrons emitted during radioactive decay. An endpoint energy positron from ^{18}F decay (633 keV) has $\gamma = 2.24$ and $\beta = 0.89$; the most probable energy (250 keV) corresponds to $\gamma = 1.49$ and $\beta = 0.74$. Note that, for the most probable kinetic energy, $\beta = 0.74$ is just below the threshold for producing Cerenkov radiation in water with $n = 1.33$ (since $\beta n < 1$). The spectrum of emitted positron energies for ^{18}F is shown in figure 2. For ^{18}F, only 47 per cent of the decays produce a positron with an energy above the Cerenkov threshold in water. In contrast, ^{90}Y, a β^--emitter used for radionuclide therapy, has a higher endpoint energy (2.28 MeV), and 90 per cent of the emitted electrons are above the Cerenkov threshold in water (figure 2).

A typical range of good (greater than 80%) quantum efficiency for a sensitive charge-coupled device (CCD) camera that might be used for detecting Cerenkov light is between 400 and 800 nm. Transferring the numbers above

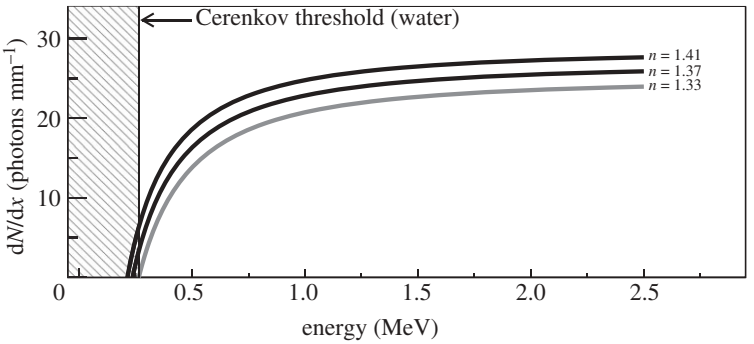

Figure 3. Number of Cerenkov photons produced per millimetre in water ($n = 1.33$) and materials with other indices of refraction ($n = 1.37$ and 1.41, typical of tissue) as a function of β-particle kinetic energy in the wavelength range 400–800 nm. The shaded area shows the region below the Cerenkov threshold for $n = 1.33$; for higher indices of refraction, the threshold is lower. Below 0.5 MeV, there is a strong dependence of the light output on the index of refraction.

into equation (2.1), we can plot the expected number of Cerenkov photons emitted per millimetre ($\mathrm{d}N/\mathrm{d}x$) within this wavelength range as a function of β-particle energy (figure 3). For an endpoint positron from ^{18}F, with an energy of 633 keV, we would therefore expect approximately 16 photons to be produced per millimetre of distance travelled. The range in water of a 633 keV positron is 2.1 mm [17]; thus an upper bound on the number of Cerenkov photons produced by an ^{18}F positron in the wavelength range 400–800 nm is 34 (16 photons per millimetre, and a distance of 2.1 mm).

However, this result is not immediately useful, as it only considers the endpoint positron energy and not the spectrum of positron energies shown in figure 2. Furthermore, each positron slows down and loses kinetic energy as it travels, producing fewer photons per millimetre than predicted, and will eventually fall below the Cerenkov threshold at some point before it stops. So, we would expect considerably less than this upper bound of 34 detectable visible light photons emitted per positron [17].

In order to model the production of Cerenkov light more accurately and to estimate its intensity and distribution in tissue, we have performed Monte Carlo simulations using the software tool GEANT4 [18,19]. These simulations model the energy spectrum of β-particles emitted from the radionuclides of interest (figure 2) as well as the changing intensity of Cerenkov emission as the particle slows in the medium. The possibility of Cerenkov light generation from energetic secondary electrons is also modelled. For these simulations, a point source of the radionuclide was located at the centre of a volume of water (with an index of refraction of 1.33 and a density of $1.0\,\mathrm{g\,cm^{-3}}$) used as the medium for generation of the Cerenkov radiation. Water and tissue have similar properties for electron/positron scattering and range, and the differences in generation and transport of Cerenkov light in tissue and water will be due to differences in index of refraction and optical scattering and absorption coefficients.

From the Frank–Tamm formula, using small step sizes (less than or equal to 50 μm), we find that the number of optical (400–800 nm) photons produced for a number of different isotopes of interest for imaging and therapy (figure 4) is in

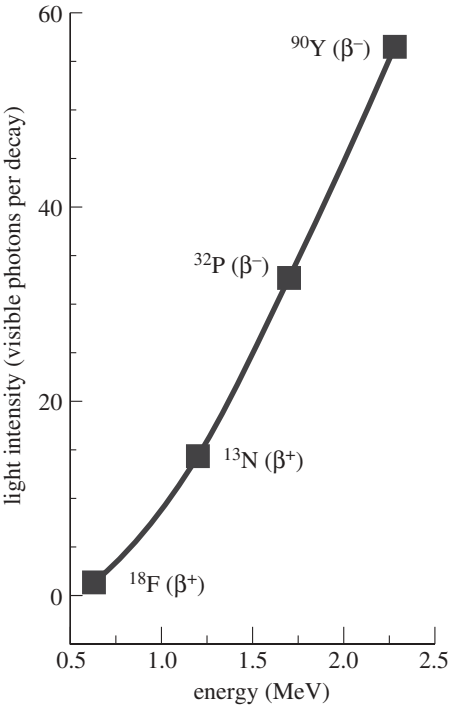

Figure 4. Simulation results showing the predicted photon yield per decay in water (in the wavelength range 400–800 nm) as a function of the β-particle endpoint energy for four radionuclides. Note that the four isotopes shown all have large branching ratios for β-particle emission.

the range 1–10^2 per decay. For ^{18}F, the average number of photons per decay is 1.4, while for ^{90}Y, the Cerenkov yield is 57 photons per decay. Simulations with varied index of refraction, elemental composition and density of tissue yielded trends similar to those shown in figure 4, with more Cerenkov radiation produced owing to a higher index of refraction. At an index of refraction of $n = 1.4$, the predicted photon yield is 2.4 photons per decay for ^{18}F and 69 photons per decay for ^{90}Y.

Typical molecular imaging studies in small animals use an injected activity of the order of 100 μCi (3.7 MBq). For ^{18}F-labelled radiotracers, this would produce a total light flux in the animal of approximately 9×10^6 photons s^{-1}. A similar activity of ^{90}Y would produce approximately 250×10^6 photons s^{-1}.

The Monte Carlo simulations also can be used to examine the spatial distribution of light emission along the path of the β-particles as they travel through water (essentially equivalent to tissue). Figure 5*a* shows several superimposed representative tracks for β-particles emitted from ^{18}F and ^{90}Y, and the point along the track at which the energy of the β-particle drops below the Cerenkov threshold. Analysing the spatial distribution of the light production over a large number of decays (10^4) by computing the root mean square (r.m.s.) spread, we find that the light is confined to a 2 mm area (r.m.s.) for even the most energetic β-emitter considered (figure 5*b*). For ^{18}F, with its low endpoint energy, the r.m.s. light spread is only 0.3 mm.

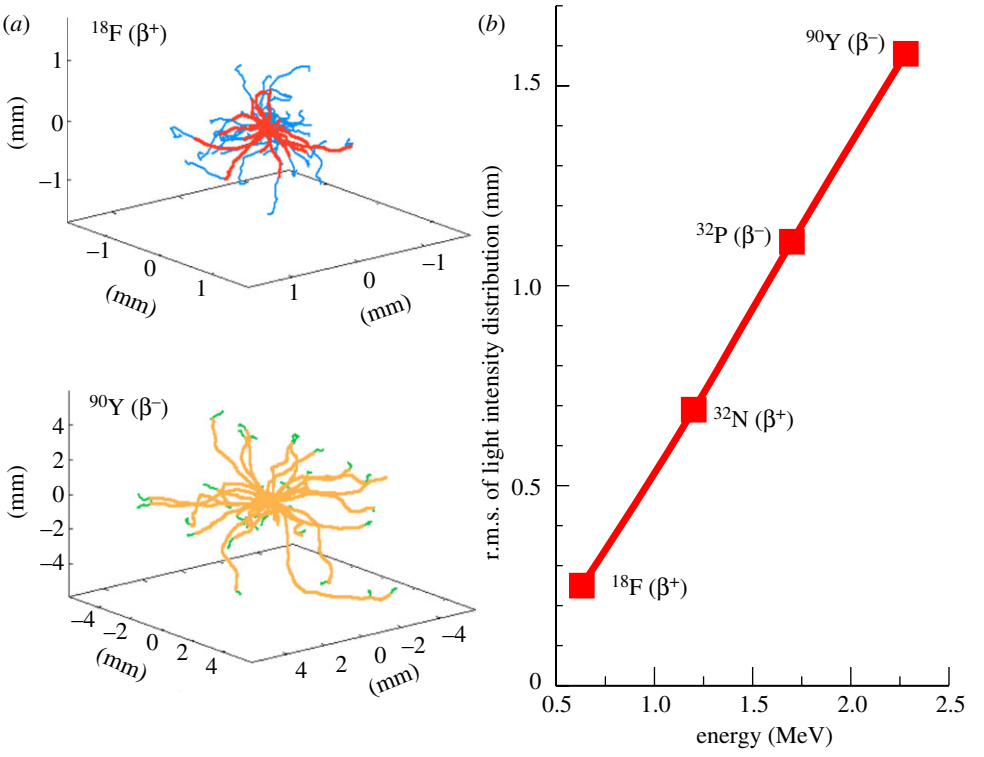

Figure 5. (*a*) Monte Carlo simulation of several β-particle tracks emanating from a point source of ^{18}F (top) and ^{90}Y (bottom) in water. Note that they are shown on different spatial scales for clarity. The change in colour in the tracks indicates the location at which the energy of the β-particle drops below the Cerenkov threshold. Some β-particles are emitted with energies below the Cerenkov threshold and therefore never produce light. This is particularly common for ^{18}F (figure 2). (*b*) Simulation results showing the predicted r.m.s. distribution in Cerenkov light production as a function of the β-particle endpoint energy for four radionuclides.

These results demonstrate the potential spatial resolution achievable with Cerenkov imaging. In practice, in any optically thick specimen, light scattering typically dominates achievable spatial resolution. However, there may be applications for Cerenkov imaging that involve surface imaging (endoscopic or catheter-based approaches, and ocular or skin imaging), where optical scattering is reduced and spatial resolution approaching these values may be achieved.

(*a*) In vitro *measurements*

Cerenkov light is detectable by a sensitive CCD camera, such as those present in several commercially available small-animal optical imaging systems. Owing to the relatively low levels of signal, cameras and systems optimized for bioluminescence imaging are typically most successful in observing Cerenkov radiation. We have used an IVIS 100 imaging system (Caliper Life Sciences, Hopkinton, MA, USA) for the measurements presented here.

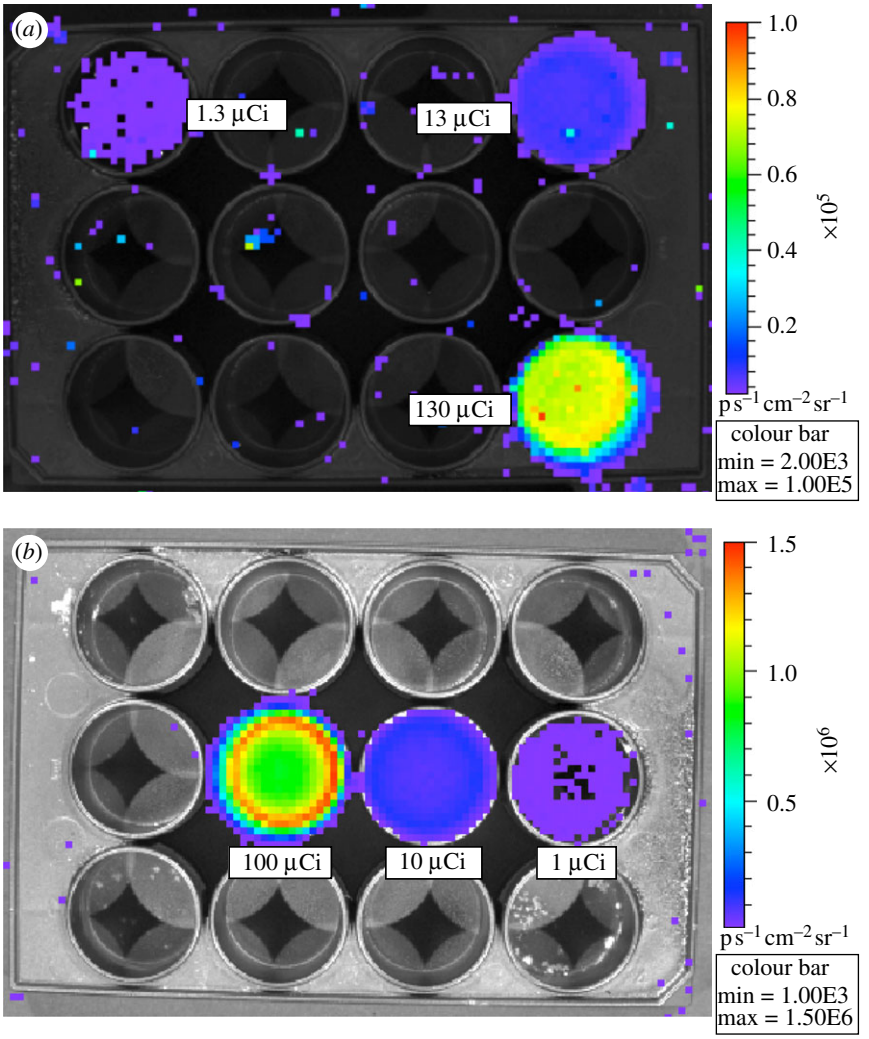

Figure 6. Well plate images. (*a*) Serial dilutions (130, 13 and 1.3 µCi) of ^{18}F; exposure time 300 s, aperture setting $f/1$, large binning. Note the occurrence of occasional 'hot pixels'—a background caused by direct interactions of 511 keV annihilation photons in the CCD. These remain after the system correction for cosmic ray interactions is applied. (*b*) Serial dilutions (100, 10 and 1 µCi) of ^{90}Y; exposure time 30 s, aperture setting $f/1$, large binning. Both images were acquired with the 15 cm field of view (position B). Note the different colour scales, as the ^{90}Y wells are much brighter. (The colour scale units of radiance are photons per second per square centimetre per steradian.)

One method to study Cerenkov luminescence imaging (CLI) in an *in vitro* environment is to acquire images of radionuclides in solution in a well plate, as shown in figure 6 for ^{18}F and ^{90}Y in 2 ml of water solution. Images of light emission from radionuclides in a solution are easily acquired with exposure times of seconds to a few minutes. Note the occurrence of occasional 'hot pixels' in figure 6*a*, a background caused by direct interactions of 511 keV annihilation

photons produced by positrons emitted from ^{18}F in the CCD chip, producing a high signal in a single pixel. These events occur across the field of view, even when the activity source is localized, because the 511 keV gamma rays are obviously not focused by the optics of the imaging system. This only becomes a practical problem when high amounts of activity are in the field of view. Even then, most CCD cameras have a cosmic ray rejection mode that can be effective in removing these events. ^{90}Y (figure 6*b*) does not show this background, as it is a fairly pure β^--emitter and does not produce any significant numbers of gamma rays or X-rays that interact directly in the CCD chip.

Drawing a region of interest around the wells in figure 6 and using the calibrated and therefore quantitative results from the imaging system software (LivingImage 3.1, Caliper Life Sciences), we can experimentally determine the number of emitted photons per second. Although the software was developed to support bioluminescence and fluoresence applications, it is also applicable to the measurement of visible light produced by the Cerenkov effect. Given that the activity in each well is known, we can use these results to measure the numbers of observed photons per decay and compare these with the Monte Carlo predictions presented in figure 4.

From our simulation results given above, we expect a theoretical number of visible light Cerenkov photons of 1.4 per decay for ^{18}F and 57 per decay for ^{90}Y. Accounting for experimental factors (geometry, camera quantum efficiency and index of refraction effects), we expect to measure a factor of 2 less than (i.e. 50%) this light yield in a water solution in well plates, leading to a predicted light yield of 0.73 photons per decay for ^{18}F and 28 photons per decay for ^{90}Y. Our experimental results give a measured intensity of 0.78 photons per decay for ^{18}F and 23.7 photons per decay for ^{90}Y, and are thus in good qualitative agreement with predictions. In the case of ^{90}Y, the underestimation is possibly due to escape of energetic β-particles from the surface of the well plate before their energy has dropped below the Cerenkov threshold. Residual differences may also be due to assumptions made in the manufacturer's calibration of the imaging system, the lack of precise information on the quantum efficiency of the CCD camera in the IVIS 100 system, and the difficulty in modelling several factors (reflections from the side of the wells, optical absorption in the wells, effects of refractive index, optical transmission through lenses and filters) in the experimental setup.

Experimentally, the optical photon intensity is found to be greater with higher-energy β-emitters, is proportional to the radionuclide activity and increases as expected with the refractive index of the medium. We have also verified that the spectral characteristics of the signal follow a $1/\lambda^2$ relationship as expected for Cerenkov light [7]. Other researchers have performed well plate (or microcentrifuge tube) measurements with similar results [8–10]. A variety of biomedically relevant radionuclides have now been studied. Overall, the results of these studies are consistent with the production of Cerenkov radiation.

Radionuclides that decay by α-particle emission should not in principle produce Cerenkov light. The heavy α-particles do not have sufficient velocity to meet the threshold for Cerenkov radiation. However, light emission from the α-emitter ^{225}Ac has been observed [10]. This is probably due to some of the daughter products of ^{225}Ac, primarily ^{213}Bi, which decays by β-emission and therefore can produce Cerenkov light.

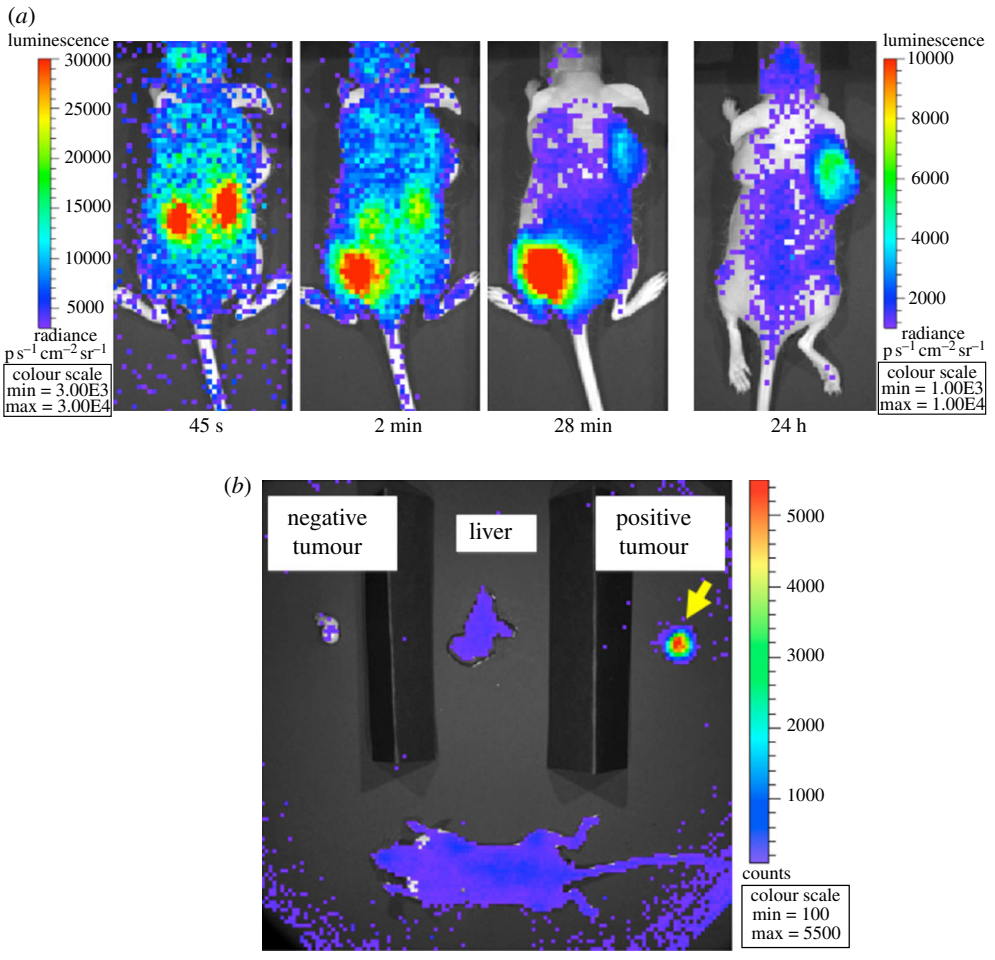

Figure 7. (*a*) *In vivo* study with engineered antibody reporter gene. The SCID mouse has a tumour expressing an engineered antibody reporter on its right shoulder. The injected dose (tail vein) of the reporter probe was 8 µCi ^{90}Y-AABD. The left colour scale is for the three leftmost images; the right colour scale is for the rightmost image. Acquisition time of the images was (left to right) 15, 30, 120 and 300 s. The images depict the changing probe biodistribution with time (clearance through kidneys into bladder) and show no apparent signal in the control tumour on the left shoulder. (*b*) *Ex vivo* biodistribution images of the animal shown in part (*a*) at 24 h verifying specific accumulation of the probe in the positive tumour with very little non-specific binding in the rest of the body (in agreement with *in vivo* imaging at the same time point).

(*b*) In vivo *studies*

To serve as illustration of the potential utility of CLI for *in vivo* molecular imaging applications, we performed a proof-of-concept animal study. A SCID (severe combined immuno-deficient) hairless outbred (SHO) mouse (Charles River) received bilateral subcutaneous injections of 3×10^6 U87 (glioma) cells suspended in 100 µl phosphate-buffered saline to the subscapular regions. Injected cells were either U87/DAbR1 (right shoulder), which stably express the DOTA Antibody Reporter-1 [20] (DOTA = 1,4,7,10-tetraazacyclododecane-*N*,*N*′,*N*″,

N'''-tetraacetic acid), or the parental U87 (left shoulder), which lack reporter expression. Animals were cared for and monitored according to IACUC-approved protocols.

Four weeks post-injection, CLI was conducted. The mouse was anaesthetized with 2 per cent isoflurane (isoflurane was maintained throughout the imaging protocol) and was injected via tail vein with 8 µCi of ^{90}Y-labelled (*S*)-2-(4-acrylamidobenzyl)-DOTA (^{90}Y-AABD). Images were then acquired dynamically with the IVIS 100 system using $f/1$, field of view B, large binning, with exposure times ranging from 15 s shortly after injection to 300 s at later time points. Figure 7*a* shows images acquired at different time points with this animal, with excellent specific binding in the positive tumour, and persistence of the signal for 24 h. The biodistribution apparent from the *in vivo* images was verified by sacrificing the mouse following the 24 h *in vivo* image, removing its liver and the two tumours, and imaging those tissues *ex vivo* along with the remaining mouse body (figure 7*b*).

The DAbR1/^{90}Y-AABD reporter system has previously been used for PET imaging using the radionuclide ^{86}Y [20]. However, ^{90}Y had not previously been used in this system, as the only imaging method available is detection of its very low-yield bremsstrahlung radiation using a gamma camera. This study illustrates the ability of CLI to image such a reporter system *in vivo* using ^{90}Y, a radionuclide of therapeutic relevance, with excellent images obtained with short acquisition times and with a very low injected dose of the probe. For comparison, a typical small-animal PET study will use an injected dose of 100 µCi and an acquisition time of 600–900 s. The use of CLI for dynamic imaging for pharmacokinetics studies will of course require balancing of injected dose, pixel binning and frame acquisition rate for the particular radiotracer. We are using this model system and CLI to evaluate different candidate probe chemistry and formulations for their uptake and clearance properties, and we find that CLI is an efficient modality for obtaining semi-quantitative *in vivo* biodistribution results.

Other groups have performed similarly successful and illustrative *in vivo* CLI mouse studies using ^{18}F-fluorodeoxyglucose [9,21], a variety of ^{18}F-, ^{131}I- and ^{90}Y-labelled probes [8], and a monoclonal antibody labelled with ^{89}Zr [10]. While further research is ongoing to fully characterize CLI, given the growing number of published studies, and the widespread availability of optical imaging instrumentation capable of detecting the signals, CLI should now be considered a modality for practical use in small-animal molecular imaging.

3. Discussion

In terms of ongoing development, we are working to better understand the quantitative characteristics of the Cerenkov signal both *in vitro* and *in vivo*. A clever idea to increase the Cerenkov signal *in vivo* is to use an exogenous probe or fluorescent protein with wavelength-shifting properties to shift some of the shorter-wavelength Cerenkov light to more penetrating longer wavelengths; this possibility has already been demonstrated by three groups [22–24]. Quantum dots are particularly promising in this regard, as they have strong absorption in the blue region of the spectrum where the Cerenkov signal is strongest, and can emit far into the red where tissue penetration is very good.

Furthermore, abundant endogenous fluorophores may also play a role in modifying the spectrum of the emitted Cerenkov light. While the fluorescent emission peaks of many endogenous fluorophores are often too far to the blue end of the spectrum to be of first-order use for *in vivo* applications, shifting the intensity of some of the continuous spectrum CLI optical signal to longer wavelengths can only help with tissue penetration and may help with the overall detection sensitivity when including quantum efficiency considerations.

Cerenkov light also has the potential to be used as an internal light source for activating photodynamic therapy or for photoactivation of drugs or drug-delivery vehicles. Many of these approaches require the delivery of energetic photons in the blue/UV part of the spectrum, and when using external light sources, only superficial tissues can be accessed. Beta-emitting radionuclides have the potential to deliver blue/UV light deep inside the body via their Cerenkov emission, and using targeted radiotracers it may be possible to deliver that light to quite specific locations. First studies on the use of radiotracer-delivered Cerenkov light for photoactivation have already been published [25].

We also note that, by measuring the emitted light from several views of the mouse, it is possible to reconstruct three-dimensional images of the Cerenkov light distribution using techniques analogous to those used for bioluminescence tomography. First tomographic studies of Cerenkov luminescence have recently been published [26–28]. Given the nature of light transport *in vivo*, CLI in general and CLI tomography in particular will be much more successful for radiotracers that have a high-contrast uptake in the tissues or cells of interest. The presence of non-specific probe accumulation, for example, 2-[^{18}F]fluoro-2-deoxy-D-glucose (^{18}F-FDG) in an animal bladder, can confound the ability to image a tumour or other organ nearby.

In theory, Cerenkov luminescence also can be used to image radiotracers administered in cell culture or bound to tissue slices. However, the low optical signal per cell, plus the fact that there will be some blurring of the image due to the range of the electrons or positrons (figure 5) in the culture medium or tissue slice, will probably make high-resolution Cerenkov luminescence microscopy difficult.

One also can envision translational applications. While optical scattering will severely limit the use of CLI in large volumes of tissues, imaging of superficial and accessible tissues, such as the skin, eyes and mouth, as well as surfaces that can be accessed by endoscopes (e.g. throat, colon, oesophagus, and so on) or catheters (blood vessels, including atherosclerotic plaques) should be possible. Intra-operative imaging of tumour resection or other surgical procedures also may be possible. The fact that a large number of PET radiotracers for many different biological targets have already been safely used in patients and volunteers makes this quite attractive. However, the challenges are quite formidable, requiring a near-zero light background to measure the very faint Cerenkov signals, and once again, the achievable spatial resolution also will be limited by a combination of the β-particle range and light scattering in tissue.

A further important consideration is that the conversion of the β-particle energy to Cerenkov light is an extremely inefficient process. For ^{18}F, the conversion efficiency (the ratio of the total energy released as visible photons to the kinetic energy of the particle) is of the order of 1×10^{-5}. Therefore, for applications involving imaging of a surface, or a signal very near a surface (such

as some of the translational applications and tissue-level interrogations proposed in the preceding two paragraphs), it may prove better to image the β-particles themselves. Each β-particle can produce many thousands of scintillation photons or electron–hole pairs in a radiation detector, thus providing a much more robust signal than CLI. This factor should be considered when proposing CLI for such applications.

To date, small-animal imaging appears to be the most appropriate niche for CLI applications. It involves imaging of tissue volumes that exclude direct detection of the β-particles themselves, yet are relatively transparent to the Cerenkov light emitted at longer wavelengths. For such applications, CLI appears to be a sensitive and useful new tool for *in vivo* imaging studies, supported by the large installed base of small-animal optical imaging instruments capable of detecting the CLI signals.

4. Conclusion

We have characterized the intensity and spatial distribution of the signal arising from the new hybrid method of CLI. It is now well established that this technique can be used for imaging β-emitting radionuclides using optical imaging of the Cerenkov light emitted as the β-particles pass through tissue. Even low-energy β-emitters (e.g. ^{18}F) produce sufficient light for detection *in vivo* with reasonable activities. Higher-energy β-emitters (e.g. ^{90}Y) produce significant amounts of visible light with only a few microcuries of injected activity *in vivo*. As this light is emitted only close to the source of the β-particle, it allows the distribution of the β-emitting radionuclide to be imaged. CLI uniquely provides a new and potentially very sensitive method to image non-invasively pure β^--emitting radionuclides, such as ^{90}Y, that are being developed for targeted radionuclide therapies (e.g. ^{90}Y-ibritumomab tiuxetan (Zevalin)). Currently, these can only be imaged via the very weak bremsstrahlung signals produced in tissue and this requires very high (often therapeutic) levels of activity for detection. Thus, potential applications for CLI include: imaging of PET and many single-photon emission computed tomography (SPECT) radiotracers on widely available commercial optical imaging systems; and guiding the development of therapeutic β^--emitters that cannot be readily imaged by other means.

The authors would like to thank Dr Claude Meares (Department of Chemistry, UC Davis) and the members of his laboratory (Tolu Aweda, Vahid Eskandari and Heather Beck) for synthesizing the probe for the engineered antibody reporter gene model system. The antibody reporter plasmid was a kind gift of Dr Anna Wu (UCLA). The authors also thank David Kukis, Michelle Connell and Doug Rowland of the Center for Molecular and Genomic Imaging, UC Davis, for assistance with the animal handling and radiochemistry for the *in vivo* studies. This research was funded by NIH Grant R21 CA143098.

References

1 Massoud, T. F. & Gambhir, S. S. 2003 Molecular imaging in living subjects: seeing fundamental biological processes in a new light. *Genes Dev.* **17**, 545–580. (doi:10.1101/gad.1047403)

2 Sandhu, G. S., Solorio, L., Broome, A.-M., Salem, N., Kolthammer, J., Shah, T., Flask, C. & Duerk, J. L. 2010 Whole animal imaging. *Wiley Interdiscipl. Rev. Syst. Biol. Med.* **2**, 398–421. (doi:10.1002/wsbm.71)

3 Krucker, T. & Sandanaraj, B. S. 2011 Optical imaging for the new grammar of drug discovery. *Phil. Trans. R. Soc. A* **369**, 4651–4665. (doi:10.1098/rsta.2011.0300)
4 Rice, B. W., Cable, M. D. & Nelson, M. B. 2001 *In vivo* imaging of light-emitting probes. *J. Biomed. Opt.* **6**, 432–440. (doi:10.1117/1.1413210)
5 Shaner, N. C., Campbell, R. E., Steinbach, P. A., Giepmans, B. N., Palmer, A. E. & Tsien, R. Y. 2004 Improved monomeric red, orange and yellow fluorescent proteins derived from *Discosoma* sp. red fluorescent protein. *Nat. Biotechnol.* **22**, 1567–1572. (doi:10.1038/nbt1037)
6 Bremer, C., Ntziachristos, V. & Weissleder, R. 2003 Optical-based molecular imaging: contrast agents and potential medical applications. *Eur. Radiol.* **13**, 231–243. (doi:10.1007/s00330-002-1610-0)
7 Robertson, R., Germanos, M. S., Li, C., Mitchell, G. S., Cherry, S. R. & Silva, M. D. 2009 Optical imaging of Cerenkov light generation from positron-emitting radiotracers. *Phys. Med. Biol.* **54**, N355–N365. (doi:10.1088/0031-9155/54/16/N01)
8 Liu, H., Ren, G., Miao, Z., Zhang, X., Tang, X., Han, P., Gambhir, S. S. & Cheng, Z. 2010 Molecular optical imaging with radioactive probes. *PLoS ONE* **5**, e9470. (doi:10.1371/journal.pone.0009470)
9 Spinelli, A. E., D'Ambrosio, D., Calderan, L., Marengo, M., Sbarbati, A. & Boschi, F. 2010 Cerenkov radiation allows *in vivo* optical imaging of positron emitting radiotracers. *Phys. Med. Biol.* **55**, 483–495. (doi:10.1088/0031-9155/55/2/010)
10 Ruggiero, A., Holland, J. P., Lewis, J. S. & Grimm, J. 2010 Cerenkov luminescence imaging of medical isotopes. *J. Nucl. Med.* **51**, 1123–1130. (doi:10.2967/jnumed.110.076521)
11 Cerenkov, P. A. 1937 Visible radiation produced by electrons moving in a medium with velocities exceeding that of light. *Phys. Rev.* **52**, 378–379. (doi:10.1103/PhysRev.52.378)
12 Jelley, J. V. 1955 Cerenkov radiation and its applications. *Br. J. Appl. Phys.* **6**, 227–232. (doi:10.1088/0508-3443/6/7/301)
13 Belcher, E. H. 1953 The luminescence of irradiated transparent media and the Cerenkov effect: I. The luminescence of aqueous solutions of radioactive isotopes. *Proc. R. Soc. Lond. A* **216**, 90–102. (doi:10.1098/rspa.1953.0009)
14 Elrick, R. H. & Parker, R. P. 1968 The use of Cerenkov radiation in the measurement of beta-emitting radionuclides. *Int. J. Appl. Radiat. Isot.* **19**, 263–271. (doi:10.1016/0020-708X(68)90023-9)
15 Cho, J., Taschereau, R., Olma, S., Liu, K., Chen, Y.-C., Shen, C. K., van Dam, R. M. & Chatziioannou, A. F. 2009 Cerenkov radiation imaging as a method for quantitative measurements of beta particles in a microfluidic chip. *Phys. Med. Biol.* **54**, 6757–6771. (doi:10.1088/0031-9155/54/22/001)
16 Eisberg, R. M. 1961 *Fundamentals of modern physics*. New York, NY: John Wiley & Sons.
17 Ross, H. H. 1969 Measurement of β-emitting nuclides using Cerenkov radiation. *Anal. Chem.* **41**, 1260–1265. (doi:10.1021/ac60279a011)
18 Agostinelli, S. *et al.* 2003 GEANT4: a simulation toolkit. *Nucl. Instrum. Meth. A* **506**, 250–303. (doi:10.1016/S0168-9002(03)01368-8)
19 Allison, J. *et al.* 2006 GEANT4 developments and applications. *IEEE Trans. Nucl. Sci.* **53**, 270–278. (doi:10.1109/TNS.2006.869826)
20 Wei, L. H. *et al.* 2008 Engineered antibody fragments with infinite affinity as reporter genes for PET imaging. *J. Nucl. Med.* **49**, 1828–1835. (doi:10.2967/jnumed.108.054452)
21 Boschi, F., Calderan, L., D'Ambrosio, D., Marengo, M., Fenzi, A., Calandrino, A., Sbarbari, R. & Spinelli, A. E. 2011 *In vivo* ^{18}F-FDG tumour uptake measurements in small animals using Cerenkov radiation. *Eur. J. Nucl. Med. Mol. Imag.* **38**, 120–127. (doi:10.1007/s00259-010-1630-y)
22 Liu, H., Zhang, X., Xing, B., Han, P., Gambhir, S. S. & Cheng, Z. 2010 Radiation-luminescence-excited quantum dots for *in vivo* multiplexed optical imaging. *Small* **6**, 1087–1091. (doi:10.1002/smll.200902408)
23 Dothager, R. S., Goiffon, R. J., Jackson, E., Harpstrite, S. & Piwnica-Worms, D. 2010 Cerenkov radiation energy transfer (CRET) imaging: a novel method for optical imaging of PET isotopes in biological systems. *PLoS ONE* **5**, e13300. (doi:10.1371/journal.pone.0013300)

24 Lewis, M. A., Kodibagkar, V. D., Oz, O. K. & Mason, R. P. 2010 On the potential for molecular imaging with Cerenkov luminescence. *Opt. Lett.* **35**, 3889–3891. (doi:10.1364/OL.35.003889)
25 Ran, C., Zhang, Z., Hooker, J. & Moore, A. In press. *In vivo* photoactivation without 'light': use of Cherenkov radiation to overcome the penetration limit of light. *Mol. Imag. Biol.* (doi:10.1007/s11307-011-0489-z).
26 Li, C., Mitchell, G. S. & Cherry, S. R. 2010 Cerenkov luminescence tomography for small-animal imaging. *Opt. Lett.* **35**, 1109–1111. (doi:10.1364/OL.35.001109)
27 Hu, Z. *et al.* 2010 Experimental Cerenkov luminescence tomography of the mouse model with SPECT imaging validation. *Opt. Express* **18**, 24 441–24 450. (doi:10.1364/OE.18.024441)
28 Zhong, J. H., Tian, J., Yang, X. & Qin, C. H. 2011 Whole-body Cerenkov luminescence tomography with the finite element SP3 method. *Ann. Biomed. Eng.* **39**, 1728–1735. (doi:10.1007/s10439-011-0261-1)